ASIAN JOURNAL OF CIVIL ENGINEERING (BHRC) VOL. 15, NO. 3 (2014)
PAGES 391-410

EXPERIMENTAL AND ANALYTICAL INVESTIGATION ON BOND PERFORMANCE OF THE INTERFACIAL DEBONDING IN FLEXURAL STRENGTHENED RC BEAMS WITH CFRP SHEETS AT TENSILE FACE

A. Sadrmomtazi*[1], H. Rasmi Atigh[1] and J. Sobhani[2]
[1]Faculty of Engineering, University of Guilan, Rasht, Iran.
[2]Department of Concrete Technology; Road, Housing & Urban Development Research Center (BHRC), Tehran, Iran.

Received: 27 June 2013 ; **Accepted:** 24 November 2013

ABSTRACT

Externally bonding of fiber reinforced (FRP) sheet to reinforced concrete (RC) beams has become a popular flexural strengthening method in recent years. The ultimate flexural strength of those strengthened beams can be improved efficiently, but it is often prevented by premature failure modes, such as sheets end interfacial debonding. This paper proposes an effective method to prevent sheets end interfacial debonding. Hence, an experimental and analytical study conducted to verify the efficiency of the proposed method. Therefore, nine concrete beams with dimensions of 100 mm width, 160 mm height and 1200 mm length were manufactured and tested. Eight specimens were strengthened in flexure with various numbers of CFRP layers and different sheets end strengthening methods. From the test results of this study it is conducted that the design guidance of ACI 440.2R-02 and ISIS Canada overestimates and the developed method by Toutanji et al. underestimates the flexural strength of CFRP strengthened RC beams at yielding. Also, applying the proposed method to sheets end strengthening, prevented sheets end interfacial debonding and increased load carrying capacity of those strengthened beams by 26% and 32%. The ductility (i.e. Δ_u⁄Δ_y) of those strengthened beams increased by 77% and 90%.

Keywords: Flexural strengthening; reinforced concrete beams; debonding; FRP; CFRP.

* E-mail address of the corresponding author: alisadrmomtazi@yahoo.com (A. Sadrmomtazi)

Abbreviations

A_s	Cross-sectional area of tension steel reinforcement
A_s	Cross-sectional area of compression steel reinforcement
A_f	Cross-sectional area of FRP sheet
b	Width of rectangular crosses section
h	Beam height
C_E	Environmental-reduction factor
d, d	Depth of centroid of tension and compression steel reinforcement from extreme compression fiber
d_f	Depth of FRP reinforcement
E_f	Modulus of elasticity of FRP material
E_c	Modulus of elasticity of concrete
E_s	Modulus of elasticity of steel
f_c	Compressive strength of concrete
f_y	Yielding strength of compression steel
I_{cr}	Moment of inertia of the cracked section based on transformed area method
I_{cr}	Moment of inertia of the cracked section without tension steel
K_m	Bond-dependent coefficient for flexure
t_f	Thickness of FRP sheets
β	Ratio of the depth of the equivalent rectangular stress block to the depth of the neutral axis
ε_{fe}	Effective design strain for FRP sheet
ε_{fu}	Specified rupture strain for FRP sheet
ε_s	Strain level in the tensile steel reinforcement
ε_s	Strain level in the compressive steel reinforcement
ε_y	Strain corresponding to the yield strength of steel reinforcement
ε_{frp}	Strain in FRP sheet
γ	Multiplier on f_c to determine the intensity of an equivalent rectangular stress distribution for concrete
φ_s	Strength reduction factor for reinforcing bar
φ_{frp}	Strength reduction factor for FRP materials
σ_s	Stress in tensile steel at ultimate condition
σ_s	Stress in compressive steel at ultimate condition

1. INTRODUCTION

There are a number of reasons to increase the load carrying capacity of a structure in service. The reasons are mainly related to changes of structure utilization, repair of defects, prevention of damages caused by earthquakes and meeting of changed standards or specifications. In the past, the increase in strength has been provided by casting additional

reinforced concrete, dowelling in additional reinforcement or externally post-tensioning the structure. More recently, attaching steel plates to the surface of the tension zone by use of adhesives and bolts has been used to strengthen concrete structures [1-4]. Over the past decades, this strengthening method has become an accepted engineering technique around the word, due to the well-known advantages of FRP composites usage over other materials usage such as minimum increase in structural size and weight, ease of site handling, their high strength/stiffness-to-weight ratio and excellent resistance against chemicals and environmental conditions. In an ideal manner, an RC beam, flexural strengthened with FRP composites in tensile face, should fail by either the crushing of the compressive concrete or the tensile rupture of the FRP composites. In fact, debonding of FRP composites from the RC beam and concrete cover separation, in a number of different modes and situations, controls the strength in the most cases, unless appropriate approaches are taken to prevent such debonding failure modes [5-10].

Generally, some of the identified failure modes are: (a) flexural failure caused by FRP rupture, (b) flexural failure caused by crushing of the compressive concrete, (c) shear failure, (d) concrete cover separation, (e) plate end interfacial debonding. Among these five failure modes, the first three are the failure modes in conventional beams with some differences [11]. The other two failure modes are not found in conventional RC beams and are instead modes unique to beams bonded with a soffit plate. These modes are known as premature debonding failure modes, as they occur before the flexural failure of the section in mode (a) or (b) or the shear failure in mode (c) occurs [12]. A number of experimental and analytical studies carried out to prevent these premature failure modes and some design guidance codes including *ACI440.2R* [13] and *ISIS Canada* [14] and analytical methods including developed method by *Toutanji et al.* [15] to determine load carrying capacity of strengthened RC beams. Plate end interfacial debonding is one of the unwanted premature failures, where the soffit plate separates from concrete surface, beginning from unwrapped end of FRP composites. Shear capacity of the interfacial zone of concrete and soffit plate plays a great role in this kind of failure. Hence it seems necessary to increase the shear capacity of interfacial zone.

For this approach an experimental and analytical program is carried out to prevent of this premature rupture with some conventional ways and with a proposal method. And also load carrying capacity of strengthened RC beams resultant from an experimental program comprised with the analytical methods and the design guidance codes.

2. EXPERIMENTAL PROGRAM

2.1 Details of beams

Nine half scale RC beams, of 160 mm deep by 100 mm wide cross section, were statically tested to failure in four-point bending, as shown in Figure 1(a). All beams were 1200 mm long over 1000 mm clear span. All beams reinforced by two 10 mm diameter bottom bars (ρ=0.98%) and one 8 mm diameter top bars, as well as two 8 mm diameter vertical branches closed stirrups spaced at 60 mm (ρ_v=0.63%). The RC beams designed to fail at flexure, where the shear load carrying capacity of RC beams were much bigger than their flexural load carrying capacity. One RC beam kept without strengthening as a control beam and

eight RC beams strengthened in flexure with externally bonded CFRP fibers on the tensile face.

The process of applying CFRP fibers to the concrete face included surface preparation, epoxy resin undercoating, CFRP fiber application and epoxy resin over coating. Prior to bonding of the CFRP fibers, surface of the concrete were ground using mechanical grinder to obtain a clean sound surface, free of all contaminants, and then cleaned with high-pressure water to remove remains.

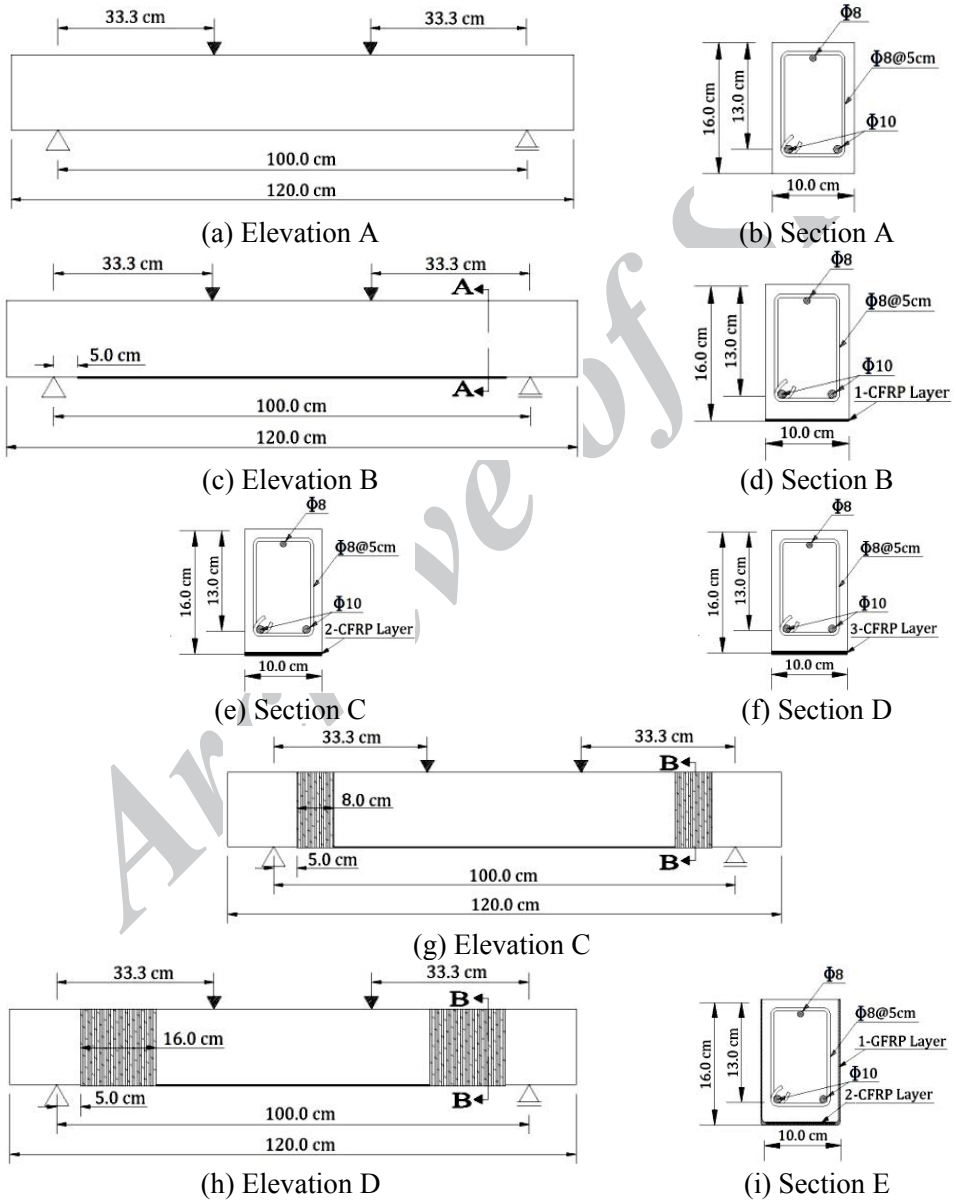

Figure 1. (a),(c),(g) and (h) Longitudinal profile of beams; (b),(d),(e),(f) and (i) cross section of beams.

2.2 Strengthening schemes

Figure 1 shows the strengthening schemes, where unlike the control beam, the other eight beams were CFRP strengthened in flexure with different number of layers and also different strengthening modes to prevent plate end interfacial debonding. One possible method to improve the resistant against sheets end interfacial debonding failure is to attach U-shape FRP stirrups over the bonded CFRP layer Figure 1(g), (h) and (i). According to recommendation of fib [3], the U-shape stirrups should be placed at the end of bonded soffit plate. In specimens Cu2-d/2 and Cu2-d two layers of CFRP fibers bonded on the bottom of the beam, at tensile face, as flexural strengthening. And then to prevent of applying additional shear stiffness, one layer of GFRP fibers (unidirectional layer in vertical direction) applied symmetrically on both sides of the beam as U-shape stirrups, with 80 mm and 160 mm wide for specimens Cu2-d/2 and Cu2-d, respectively.

The bonding stresses on CFRP-concrete interface are mainly normal and shear stresses. CFRP on bottom face of the beam, which subject to flexural strengthening, bears tensile stresses transferred through interface shear stresses and improves the bonding load carrying capacity of the beam. The interfacial normal stresses also have influence on strengthened beam behavior. At the end part of CFRP sheets where there is a truncation of CFRP, stress concentration occurs and makes the CFRP sheets debonding. Interfacial shear stresses reach their maximum at the end part of CFRP and decrease nonlinearly with the increase of distance away from CFRP sheets end. Interfacial shear stresses are much bigger than interfacial normal stresses. It is the interfacial shear stresses that result in debonding of adhesive layer [16]. Therefore, a proposal approach applied to prevent CFRP layers end interfacial debonding, where the shear capacity of interfacial zone of CFRP layer with concrete improved at the end of layers by proposal drilling scheme (DS). Hence, in specimens C1-d, C2-d and C3-d overall twenty holes drilled at the two ends of CFRP layers in length of 160 mm in eight lines with the distance of 20 mm from each other. As shown in Figure 2, these holes drilled cylindrical from the distance of 50 mm of supporting, with diameter of 8 mm and depth of 4mm.

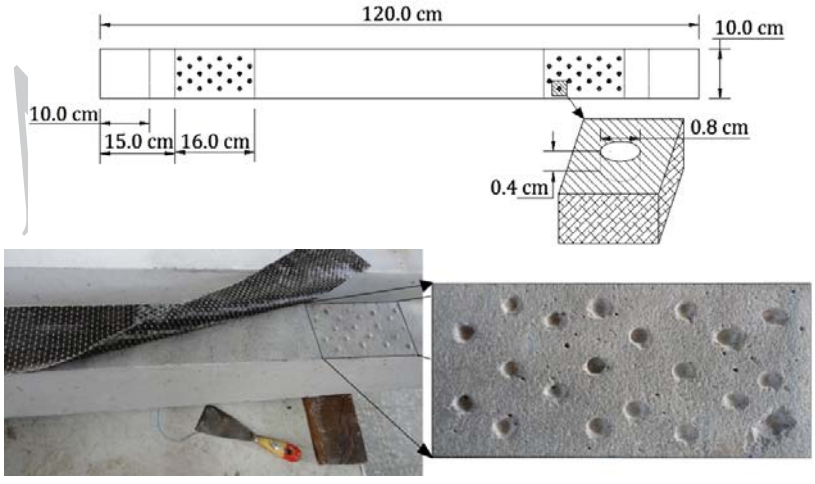

Figure 2. Bottom-longitudinal profile of beams C1-d, C2-d and C3-d

After drilling, the holes cleaned with high pressure water from remains. Then specimens kept away for two days to be dried. The process of applying CFRP sheets to the concrete surface was the same as the others, where by applying the two part epoxy-resin, the drilled holes filled completely with epoxy-resin. Then the specimens of C1-d, C2-d and C3-d strengthened with one, two and three layers of CFRP fibers in tensile face, respectively (Figure 1 c, d, e and f).

Specimens C1, C2 and C3 strengthened with one, two and three layers of CFRP fibers in tensile face, respectively, with no strengthening scheme at the ends of layers (Figure 1c, d, e and f).

2.3 Material properties

For each RC beam five 100×100×100 mm concrete cube specimens were made at the time of casting and were kept with the beams during curing. The average concrete compressive strength ($f_c^{'}$) for each beam is shown in Table 1. The relationship of cylinder strength ($f_c^{'}$) and the cube strength supposed as: $f_c^{'} = 0.85 f_{cu}$.

Table 1: Details of the simply supported beams

Specimens	$\mathbf{f_c^{'}}$ (MPa)	Tensile region strengthening		CFRP end anchorage type
		No. layers of CFRP sheets	Strengthened length (m)	
CB	40.2	-	-	-
C1	40.2	1	0.9	None
C1-d	40.2	1	0.9	Drilled at the end of layer-in length of d (DS)
C2	40.0	2	0.9	None
Cu2-d/2	40.0	2	0.9	U-wrap at the end of layer-in length of d/2
Cu2-d	40.0	2	0.9	U-wrap at the end of layer-in length of d
C2-d	40.4	2	0.9	Drilled at the end of layer-in length of d (DS)
C3	40.4	3	0.9	None
C3-d	40.4	3	0.9	Drilled at the end of layer-in length of d (DS)

In this experimental and analytical program two diameters of 10 mm and 8 mm steel bars were used. For each bar size three bar specimens were tested in tensile, the measured yield strength were 382 and 379 MPa, and maximum tensile strength were 573 and 568 MPa, respectively. The modulus of elasticity of steel bars was 2×10^5MPa.

Mechanical properties of unidirectional CFRP and GFRP fibers were obtained from the supplier and are given in Table 2.

Table 2: Mechanical properties of the FRP layers

Material	Areal weight (g/m^2)	Thickness (mm)	Ultimate tensile stress $\boldsymbol{\sigma_{fu}}$ (MPa)	Ultimate strain $\boldsymbol{\varepsilon_{fu}}$ (%)	Young's modulus $\boldsymbol{E_{fu}}$ (GPa)
CFRP	200	0.111	3900	1.66	235
GFRP	430	0.176	2700	3.72	72.4

2.4 Instrumentation

To measure the load carrying capacity of beams and their displacement at mid span and under load direction, concrete compressive strain at level of compressive steel bars and

concrete tensile strain at the level of tensile steel bars and strain of tensile steel bars at mid span, various measuring devices were applied. The measuring and monitoring devices and their location along the beam is shown in Figure 3.

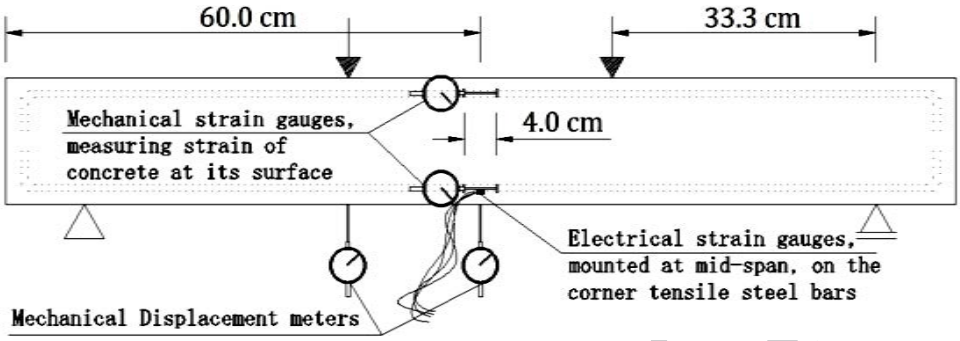

Figure 3. Deflection, concrete strain and tensile steel strain measurements

Therefore, two electrical strain gauges of 10-mm length and 120-Ohm resistance were mounted at mid span, on the corner tensile steel bars of all beams to measure the strain of tensile steel bars. And two mechanical strain gauges were mounted on the side face of concrete at level of tensile and compressive steel bars, to measure the strain of tensile concrete and compressive strain at their mounted location, respectively. The other two mechanical displacement meters applied to measure of displacement of RC beams at mid span and under the applied load direction, as shown in Figure 3.

2.5 Test setup und loading procedure

The beams were statically tested in four-point bending. The electrical strain gauges were recorded using data logging equipment and the mechanical measuring devices were recorded visually at each load increment. A view of test set up, data logging and various measuring devices is shown in Figure 4-(a).

(a) Test setup and data logging equipment

(b) Control beam

(c) Specimen C1 (d) Specimen C1-d

(e) Specimen C2 (f) Specimen C2-d

(g) Specimen Cu2-d (h) Specimen Cu2-d/2

(i) Specimen C3 (j) Specimen C3-d

Figure 4. View of test set up, data logging equipment and specimens at failure.

3. EXPERIMENTAL RESULTS

3.1 Test observations

Figure 4 shows traditional crack patterns in all tested beams at failure. As expected

previously, control RC beam failed at flexure caused by critical flexural cracks. Where the control beam had higher flexibility in comparison with CFRP strengthened beams. A summary of experimental results of the nine RC beams subjected to four-point bending test is given in Table 3. It can be seen that the yielding load values are directly related to the number of CFRP fiber layers, where the plate end strengthening schemes have no effects on the yielding load values. As the specimens C1 and C1-d have the same value of P_y (50.3 and 50.0 KN, respectively), whereas these beams strengthened with one layer of CFRP fibers, as indicates in Table 1. By increment in number of applied CFRP layers in specimens C2, Cu2-d/2, Cu2-d and C2-d the value of P_y increased to 58.0, 58.2, 58.5 and 58.3 KN, respectively, which approximately present the same values. The yielding loads of specimens C3 and C3-d were 64.0 and 64.2 KN, respectively, as these beams strengthened with three layers of CFRP fibers in flexure. Hence, it can be inferred that the same strengthening schemes in flexure lead beams to have the same yielding load. The yielding load increase is 40%, 57% and 73% for one, two and three layers of CFRP reinforcement, respectively.

Table 3: Results of tested beams including failure mode, ultimate and yielding of load and displacements at mid-span

Specimens	Failure modes	Yielding point		Failure point		$\frac{\Delta_y}{\Delta_{y-control}}$	$\frac{P_y}{P_{y-control}}$	$\frac{P_u}{P_{u-control}}$	Ductility
		P_v (KN)	Δ_v (mm)	P_u (KN)	Δ_u (mm)				Δ_u/Δ_y
CB	Flexural failure	37.0	2.30	53.00	15.20	1.00	1.00	1.00	6.60
C1	Rupture of CFRP layer	50.3	2.79	73.60	8.42	1.21	1.40	1.39	3.02
C1-d	Rupture of CFRP layer	50.0	2.69	74.00	8.42	1.17	1.35	1.40	3.13
C2	Plate end interfacial debonding	58.0	3.13	75.75	5.89	1.36	1.57	1.43	1.88
Cu2-d/2	Plate unwrapped end interfacial debonding	58.2	3.11	79.55	7.58	1.35	1.57	1.50	2.43
Cu2-d	Plate unwrapped end interfacial debonding	58.5	3.14	84.75	8.31	1.36	1.58	1.60	2.65
C2-d	Concrete cover separation	58.3	3.12	95.25	10.40	1.36	1.57	1.80	3.33
C3	Plate end interfacial debonding	64.0	3.23	71.75	4.55	1.40	1.73	1.35	1.41
C3-d	Concrete cover separation	64.2	3.22	94.75	8.64	1.40	1.73	1.79	2.68

Figure 5 presents experimental flexural rigidity, after concrete cracking the flexural rigidity decrease. As this figure shows, strengthened specimens with the same number of CFRP layers indicate the same manner in flexural rigidity. Hence, deflection at yielding of beams at mid-span depends on the flexural strengthening scheme not to the sheets end strengthening scheme. As indicated in Table 3, when the amount of CFRP reinforcement increases from one layer up to three, beams deflection at failure decreases and failure mode became more brittle, but beams deflection at tensile steel yielding increases by 21%, 36% and 40% for one, two and three layers of CFRP strengthening, respectively.

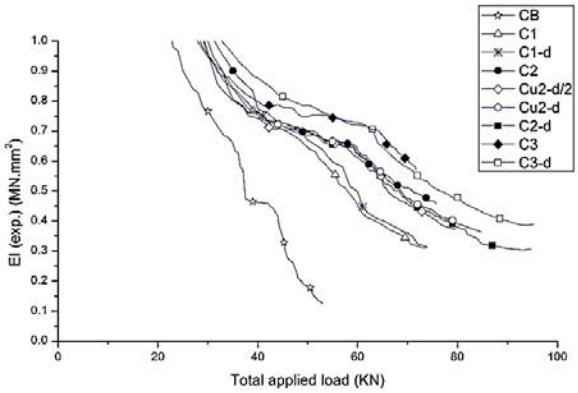

Figure 5. Experimental flexural rigidity

Increasing the applied load causes beam parts to carry higher stresses, these higher stresses makes cracking initiation in parts which are not able to bear higher stresses and lead the beams to failure. Interface of CFRP-concrete is one of the critical parts, where shear cracks makes interfacial debonding in strengthened beams, as occurred in specimens C1, C2 and C3, as shown in Figure 4-(c), (e) and (i). In specimens C1-d, C2-d, Cu2-d/2, Cu2-d and C3-d, by increasing the shear capacity of CFRP layers end, it is tried to prevent sheets end interfacial debonding. Strengthening scheme in specimens Cu2-d/2 and Cu2-d delayed interfacial debonding and also forwarded it to unwrapped end of CFRP sheets, but interfacial debonding occurred in these two specimens, as shown in Figure 4-(g) and (h). On the other hand, strengthening scheme in specimens C2-d and C3-d prevented the interfacial debonding, concrete cover separation failure mode occurred in these beams, as shown in Figure 4-(f) and (j). By increasing the number of CFRP layers, beams tended to have more brittle and stiffer manner, where the displacement values at yielding point decreased with increment in number of CFRP layers.

3.2 Deflections at mid-span and under load

Figure 6 and Figure 7 show load-deflection curves of beams at mid span and under load direction. These figures indicate that all beams have the same behavior, where each curve can be divided into three parts as: (a) from beginning of loading up to cracking of tensile concrete, (b) after cracking of tensile concrete up to the yielding of tensile steel bars and (c) yielding of tensile steel bars up to the failure point.

In part (a) the combination of concrete, steel bars and CFRP fibers carry tensile stresses. If stiffness of beam in tensile or compressive part defines as the summation of stiffness of various elements that can resist against strain, as usual, thereupon, in part (a) tensile concrete, tensile steel bars and composite fibers are the elements that constitute tensile stiffness. In part (b) where tensile concrete is cracked, one element omits from tensile stiffness, as the cracked concrete is unable to carry tensile stress. In this part tensile steel bars and CFRP fibers carry tensile stresses. Hence, at beginning point of part (b), point of A, slope of the curves changes to a lower value, in comparison with part (a). In part (c) after yielding of tensile steel bars, these bars have no proportion in load carrying of increment load. In this part CFRP fibers are the only part which participates in tensile stiffness,

therefore at point B the slope of curves again changes to lower value. In part (c) curves have the lowest slope in comparison with the other parts.

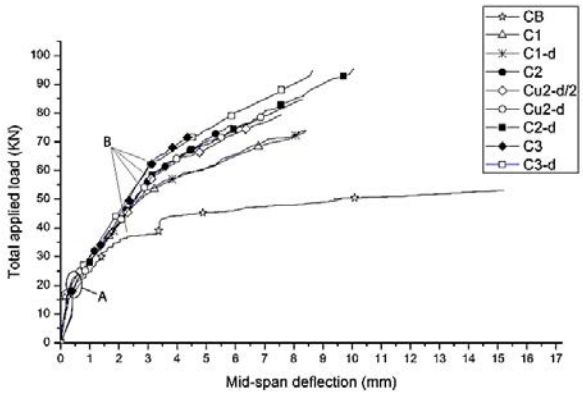

Figure 6. Total applied load versus mid-span deflection curves for test beams

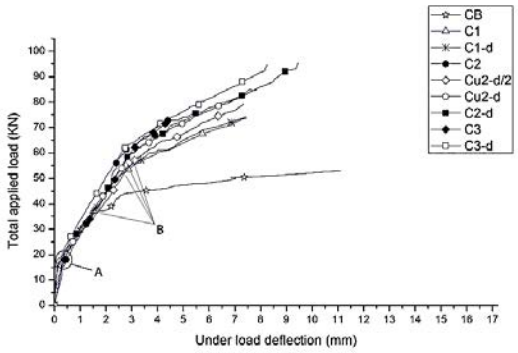

Figure 7. Total applied load versus under load deflection curves for test beams

Unlike point B, in small part after point A the slope of curves become aero. At point A which tensile concrete cracks and as the cracked concrete cannot carries tensile stresses, by losing resistance its tensile stress becomes zero. Hence at this point beams will have initial energy abandonment. This energy transmits to tensile and compressive parts of strengthened beams. Therefore, without increment in external loads, beams will face with stress increment which makes deflection, as shown in Figure 6 and Figure 7.

Whereas at point B which tensile steel bars yield, they cannot carry additional load but their tensile stress values remains constant, yet. Hence, no energy releases and no zero slopes appear in curves.

As shown in Table 3, with the increment in number of CFRP layers, in specimens C1, C2 and C3, the ductility of RC beams (Δ_u/Δ_y) is greatly reduced compared to control beam. Where, by applying sheets end strengthening scheme, the ductility of strengthened RC beams increased (specimens C2-d and C3-d compared to specimens C2 and C3, respectively).

3.3 Compressive concrete strain and tensile concrete strain

As Figure 8 indicates, behavior of control and CFRP strengthened beams are quite different in load-strain of compressive concrete curves. Due to the compressive concrete crushes in control beam, the slope of curve in control beam changes. Whereas, the compressive concrete does not crush and compressive steel bars do not yield up to failure point, the slope of curves remains constant in strengthened RC beams. Hence, in strengthened beams the relation between compressive concrete strain and applied load can be estimated by line equation with a relatively good approximation. And as the concrete compressive strain measured at level of compressive steel bars and did not measure at extreme compression fiber, the beginning point of curves is no zero.

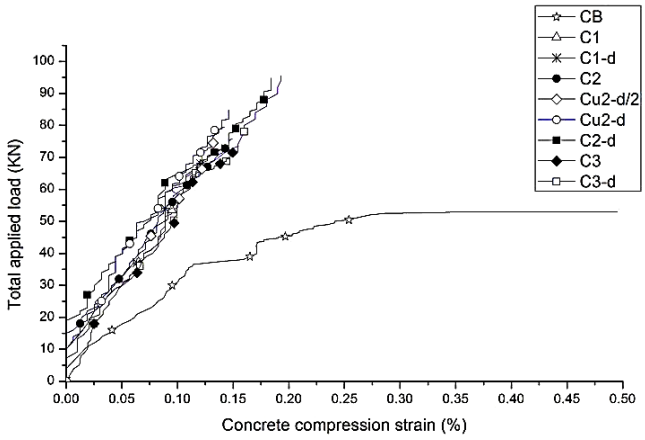

Figure 8. Total applied load versus concrete compression strain at compression steel level for test beams

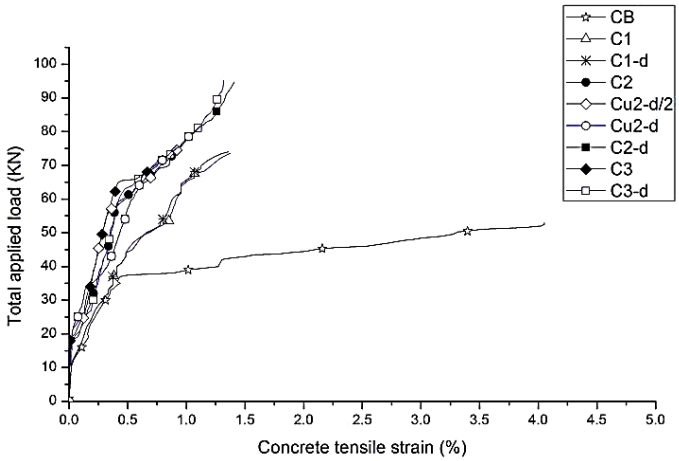

Figure 9. Total applied load versus concrete tensile strain at tensile steel level for test beams

As shown in Figure 9 Load-concrete tensile strain curves are closely similar to load-deflection curves, in behavior. As it mentioned in part 0 these curve can be divided into parts (a), (b) and (c), as explained previously. Where up to tensile concrete does not cracked the value of concrete tensile strain is negligible and is quite zero. As the tensile concrete cracks its strain increased significantly by increment in applied load. As Figure 10 indicates, concrete tensile strain variation versus applied load is much bigger than the concrete compression strain variation versus applied load. This is due to the fact that the RC beams have been designed to have flexural failure in tensile.

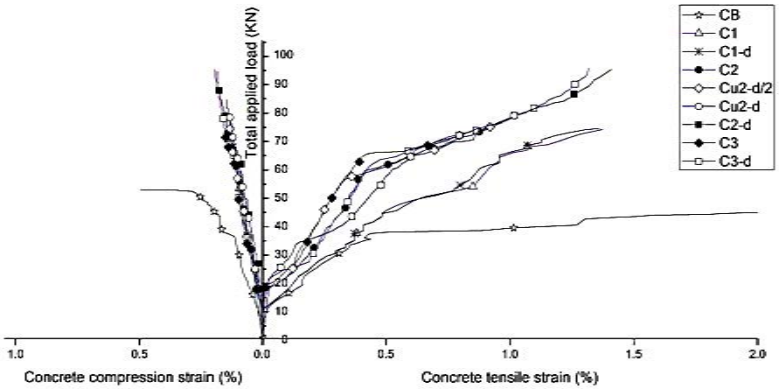

Figure 10. Total applied load versus concrete compression strain at compression steel level and concrete tensile strain at tensile steel level for test beams

4. ANALYTICAL STUDY

4.1 Proposed equation by ACI440.2R-02

ACI 440.2R-02 [13] uses a rectangular stress block similar to that used in normal reinforced concrete beams. In order to maintain a sufficient ductility the strain level in the steel at the ultimate-level state should be checked. Adequate ductility is achieved if the strain in the steel at the point of concrete crushing is at least 0.005. Therefore ACI uses a strength reduction factor calculated by equation below, where ε_s is the strain in the steel at the ultimate limit state.

$$\varphi = \begin{cases} 0.9 & \varepsilon_s \geq 0.005 \\ 0.7 + \frac{0.2(\varepsilon_s - \varepsilon_y)}{0.005 - \varepsilon_y} & \varepsilon_y < \varepsilon_s < 0.005 \\ 0.7 & \varepsilon_s \leq \varepsilon_y. \end{cases} \quad (1)$$

ACI also to prevent debonding of the FRP sheet applies limit values for ultimate strain of FRP sheet as the following equations:

$$\varepsilon_{fu} = C_E \varepsilon_{frp} \tag{2}$$

$$\varepsilon_{fe} \leq k_m \varepsilon_{fu} \tag{3}$$

$$k_m = \begin{cases} \frac{1}{60\varepsilon_{fu}}\left(1 - \frac{nE_f t_f}{360\,000}\right) \leq 0.90, & nE_f t_f \leq 180\,000 \\ \frac{1}{60\varepsilon_{fu}}\left(\frac{90\,000}{nE_f t_f}\right) \leq 0.90, & nE_f t_f > 180\,000. \end{cases} \tag{4}$$

The design flexural strength is calculated by using the following equation. An additional reduction factor ψ_f is applied to the contribution of the FRP system.

$$\varphi M_n = \varphi\left[A_s\sigma_s\left(d - \frac{\gamma c}{2}\right) + \psi_{frp}A_f E_f \varepsilon_{fe}\left(d_f - \frac{\gamma c}{2}\right) + A_s'\sigma_s'\left(\frac{\gamma c}{2} - d'\right)\right]. \tag{5}$$

4.2 Proposed equation by ISIS Canada

ISIS [14] considers a linear strain variation over the depth of section, also for ultimate bending moment, uses material strength reduction factors φ of 0.85, 0.75 and 0.6 for steel, FRP sheets and concrete. According to *ISIS*, the reinforcement ratio, ρ, calculates by considering the materials strength reduction factor.

The ultimate bending moment according to ISIS Canada is calculated by:

$$M_u = \varphi_s A_s\sigma_s\left(d - \frac{\beta c}{2}\right) + \varphi_{frp}A_f\sigma_f\left(d_f - \frac{\beta c}{2}\right) + \varphi_s A_s'\sigma_s'\left(\frac{\beta c}{2} - d'\right). \tag{6}$$

Where, $\varepsilon_{cu}' = 0.0035$

4.3 Developed equation by Toutanji et al.

Toutanji et al. [15] divided the moment deflection curves into three straight lines. The controlling points of the moment deflection curves are (Δ_{cr}, M_{cr}), (Δ_y, M_y) and (Δ_u, M_u). The yielding flexural moment and mid-span deflection at yielding calculated by equations:

$$M_y = k_1 k_2 f_c' b c^2 + A_s' E_s \varepsilon_s'(c - d') + A_s f_y(d - c) + A_f E_f \varepsilon_{frp}(h - c). \tag{7}$$

$$\Delta_y = \frac{M_y}{24E_c I_{cr}}(3L^2 - 4a^2). \tag{8}$$

where

$$k_1 = \frac{\varepsilon_c}{\varepsilon_0}\left(1 - \frac{\varepsilon_c}{3\varepsilon_s}\right) \tag{9}$$

and

$$k_2 = \frac{2}{3}\left[\frac{1-\frac{3}{8}(\varepsilon_c/\varepsilon_0)}{1-\frac{1}{3}(\varepsilon_c/\varepsilon_0)}\right]. \quad (10)$$

When the maximum moment increases from yielding moment,M_y, to ultimate moment,M_u, the mid-span deflection increases from Δ_y to Δ_u. The ultimate moment and ultimate mid-span deflection given be the following equations:

$$M_u = k_1 k_2 f_c' b c^2 + A_s' E_s \varepsilon_s' (c - d') + A_s f_y (d - c) + A_f E_f \varepsilon_{frp} (h - c). \quad (11)$$

$$\Delta_u = \frac{M_u}{24 E_c I_{cr}'} (3L^2 - 4a^2). \quad (12)$$

5. COMPARISON BETWEEN EXPERIMENTAL RESULTS AND THEORETICAL PREDICTIONS

It should be noted that, the design strength equation proposed by *ACI 440* and *ISIS Canada* have been developed based on the strength of materials up to the yielding of steel bars and/or rupture of FRP sheets with compressive concrete crushing (e.g. on condition that tensile steel bars yield, the stress level in FRP materials and compressive steel bars calculate). Hence, the calculated values according to *ACI* and *ISIS* should be compared with the test results at yielding. This is due to the fact that, as the tensile steel bars yield, FRP materials in tensile face are still bearing addition load. Thus, after yielding of tensile bars, the strengthened beams are carrying higher loads, even though the tensile bars are yielded.

Comparing the test results of all specimens with those calculated according to *ACI 440* and *ISIS Canada* show that these design codes overestimate the bending strength of strengthened beams, as shown in Figure 11. Where, as the number of CFRP layers increases the ratio of $P_{y\text{-}Test}/P_{ACI}$ or $P_{y\text{-}Test}/P_{ISIS}$ increases, as shown in Table 4. Therefore, the equations proposed by *ACI 440* and *ISIS Canada* are more appropriate in beams with less CFRP strengthening sheets.

Table 4: Comparison between test results with the calculated values by *ISIS Canada* [14] and *ACI440.2R.02* [13]

Specimens	Test				ISIS		ACI	
	P_y	Δ_y	P_u	Δ_u	P_y	P_{Test}/P_{ISIS}	P_y	P_{Test}/P_{ACI}
CB	37.0	2.3	53.0	15.2	36.1	1.02	39.3	0.94
C1	50.3	2.8	73.6	8.4	55.6	0.90	59.9	0.84
C1-d	50.0	2.7	74.0	8.4	55.6	0.90	59.9	0.83
C2	58.0	3.1	75.7	5.9	66.8	0.87	71.6	0.81
Cu2-d/2	58.2	3.1	79.5	7.6	66.8	0.87	71.6	0.81
Cu2-d	58.5	3.1	84.5	8.3	66.8	0.87	71.6	0.82
C2-d	58.3	3.1	95.2	10.4	66.8	0.87	71.6	0.81
C3	64.0	3.2	71.5	4.5	74.3	0.86	80.5	0.79
C3-d	64.2	3.2	94.7	8.6	74.3	0.86	80.5	0.80

Table 5 shows the comparison between test results with the calculated values by developed analytical method of *Toutanji et al*. In all strengthened specimens, this analytical method underestimates the deflection and load at yielding, as shown in Figure 13 and Figure 11. Where with the increment in number of CFRP layers the ratio of $P_{y\text{-}Test}/P_{y\text{-}Tout.}$ and the ratio of $\Delta_{y\text{-}Test}/\Delta_{y\text{-}Tout.}$ increase. In specimens of C1 and C1-d which rupture of CFRP sheets occurred, the ratio of $P_{u-Test}/P_{u-Tout.}$ are the same value of 0.9, as the analytical method estimates the same value of 80.4 KN for these specimens.

Table 5: Comparison between test results with the calculated values with developed method by *Toutanji et al.* [15]

Specimens	$P_{y\ Test}$	$P_{y\ Tou.}$	$P_{y\text{-}Test}/P_{y\text{-}Tou.}$	$\Delta_{y\ Test}$	$\Delta_{y\ Tou.}$	$\Delta_{y\text{-}Test}/\Delta_{y\text{-}Tou.}$	$P_{u\ Test}$	$P_{u\ Tou.}$	$P_{u\text{-}Test}/P_{u\text{-}Tou.}$	$\Delta_{u\ Test}$	$\Delta_{u\ Tou.}$	$\Delta_{u\text{-}Test}/\Delta_{u\text{-}Tou.}$
CB	37.0	41.9	0.88	2.30	2.29	1.00	53.0	-	-	15.2	-	-
C1	50.3	47.7	1.05	2.79	2.35	1.19	73.6	80.4	0.91	8.42	20.5	0.41
C1-d	50.0	47.7	1.05	2.69	2.35	1.14	74.0	80.4	0.92	8.42	20.5	0.41
C2	58.0	53.6	1.08	3.13	2.41	1.30	75.7	103.9	0.73	5.89	16.2	0.36
Cu2-d/2	58.2	53.6	1.08	3.11	2.41	1.29	79.5	103.9	0.76	7.58	16.2	0.47
Cu2-d	58.5	53.6	1.09	3.14	2.41	1.30	84.7	103.9	0.81	8.31	16.2	0.51
C2-d	58.3	53.6	1.09	3.12	2.41	1.29	95.2	103.9	0.92	10.4	16.2	0.64
C3	64.0	59.2	1.08	3.23	2.45	1.32	71.7	125.2	0.57	4.55	12.5	0.36
C3-d	64.2	59.2	1.08	3.22	2.45	1.31	94.7	125.2	0.76	8.64	12.5	0.69

In the case of ultimate load carrying capacity, the analytical method of *Toutanji* overestimates the ultimate strength of strengthened beams, as shown in Figure 12. In specimens C1, Cu2-d/2, Cu2-d and C2-d, as the applied method to sheets end strengthening improved the ratio of $P_{u\text{-}Test}/P_{u\text{-}Tout.}$ increased. Therefore, by considering ultimate load carrying capacity of strengthened beams, the analytical method of Toutanji is more appropriate in beams which suitable sheets end strengthening method is applied (e.g. drilling method which proposed and applied in this article, as shown in Figure 2). These explanations, also governs in specimens C3 and C3-d, where the ratio of $P_{u\text{-}Test}/P_{u\text{-}Tout.}$ increased in specimen C3-d in comparison with specimen C3 as the CFRP sheets end strengthened with appropriate method in specimen C3-d.

As Table 5 indicates, the ratio of $\Delta_{u\text{-}Test}/\Delta_{u\text{-}Tout.}$ increased with applying suitable method to strengthening sheet ends, as increased in specimens C2, Cu2-d/2, Cu2-d and C2-d, respectively. The ratio of $\Delta_{u-Test}/\Delta_{u-Tout.}$ proves that the analytical method developed by *Toutanji et al.* seems to be less appropriate in determination of ultimate flexural deflection of CFRP strengthened beams. Where, the aforementioned method estimated the ultimate flexural deflection twice greater than the experimental results (Figure 14).

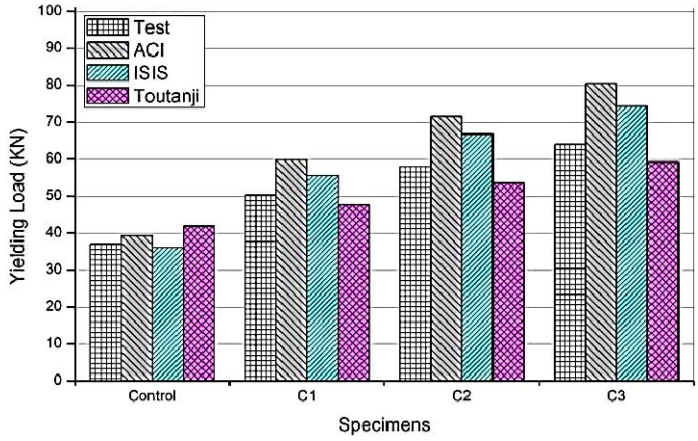

Figure 11. Comparison between experimental and analytical yielding load

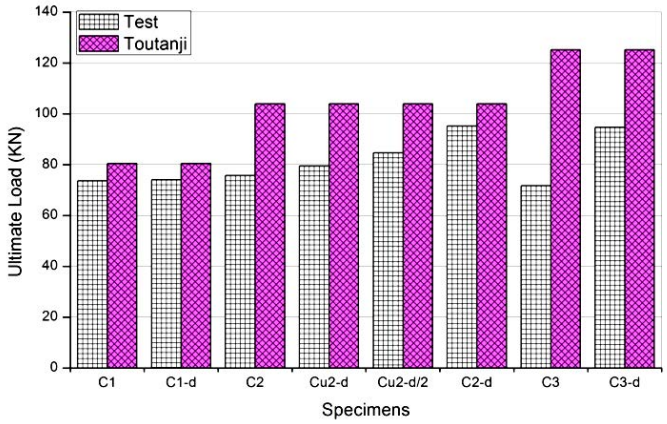

Figure 12. Comparison between experimental and analytical ultimate load

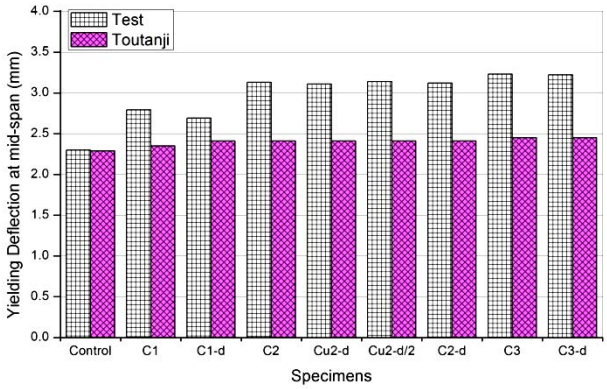

Figure 13. Comparison between experimental and analytical yielding deflection at mid-span

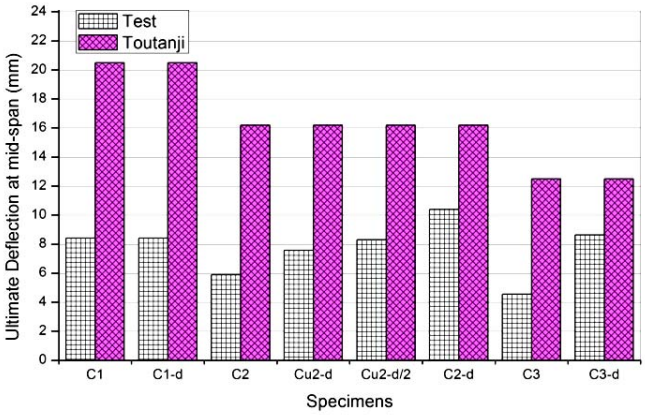

Figure 14. Comparison between experimental and analytical yielding deflection at mid-span

6. CONCLUSION

The main aim of this study was to prevent CFRP sheets end debonding failure mode, by applying U-wrap GFRP sheets and a proposal method to increase sheets end interfacial contact with concrete (nominated as DS method). Hence, an experimental and analytical study carried out where overall nine RC beams were tested under four-point bending: one control beam and eight RC beams strengthened with carbon fiber sheets in flexure. From the test results and calculated strength and deflection values, the following conclusions are drawn:

- Specimens which simply strengthened with CFRP sheets, experienced sheets end interfacial debonding, where by applying DS method, by prevention of occurrence premature failure mode of sheets end interfacial debonding, specimens faced to concrete cover separation.
- U-wrap strengthening scheme at sheets end increased load carrying capacity of strengthened beams by 12%, but it could not to prevent of sheets end interfacial debonding, where sheets end interfacial debonding occurred at sheets unwrapped ends.
- By applying DS method, load carrying capacity of strengthened beams with two and three layers of CFRP sheets increased by 26% and 32%, respectively. Also, ductility (Δ_u/Δ_y) of those strengthened beams increased by 77% and 90%, with the application of DS method.
- Unlike the flexural strengthening, the applied strengthening schemes at sheets end (U-wrap and DS method) had no effect on yielding load.
- Similar to previous studies, the flexural strength, deflection and stiffness of the strengthened beams increased compared to the control RC beam.
- The test results show that *ACI 440* and *ISIS Canada* overestimate the effect of CFRP sheets.

- As the amount of applied CFRP sheets increase, the ratios of the test load to the load calculated by *ACI 440* and *ISIS Canada* i.e. $P_{y\text{-}Test}/P_{ACI}$ and $P_{y\text{-}Test}/P_{ISIS}$increase. Therefore, the equations proposed by *ACI 440* and *ISIS Canada* could be more appropriate as the amount of CFRP sheets decreases.
- Developed method by *Toutanji et al.* underestimates the yielding load and yielding deflection, and overestimates the ultimate load and ultimate deflection of strengthened RC beams. Application of aforementioned method to estimation of ultimate deflection value is less suitable, where it estimated the ultimate flexural deflection twice greater than the experimental results.
- The results of the study which presented in this paper are part of ongoing research project being conducted at Guilan University. Future study will be focused on the prevention of premature failure mode of concrete cover separation of RC beams strengthened with FRP materials in flexure.

REFERENCES

1. Obaidat YT, Heyden S, Dahlblom O. The effect of CFRP and CFRP/concrete interface models when modeling retrofitted RC beams with FEM, *Composite Structures*, **92**(2010) 1391-8.
2. Nardone F, Lignola GP, Prota A, Manfredi G, Nanni A. Modeling of flexural behavior of RC beams strengthened with mechanically fastened FRP strips, *Composite Structures,*; **93**(2011) 1973-85.
3. International Federation for Structural Concrete Externally bonded FRP reinforcement for RC structures, Fib Bulletin 14, 2001.
4. Colotti V, Swamy RN. Unified analytical approach for determining shear capacity of RC beams strengthened with FRP, *Engineering Structructures*, **33**(2011) 827-42.
5. Yao J, Teng JG. Plate end debonding in FRP-plated RC beams-I: Experiments, *Engineering Structures*, **29**(2007) 2457-71.
6. Hollaway L, Leeming MB. *Strengthening Of Reinforced Concrete Structures: Using Externally-Bonded FRP Composites In Structural And Civil Engineering*, CRC; 1999. ISSN 0849317150.
7. Ohlers DJ, Serancino R. Design of FRP and steel plated RC structures: Retrofitting beams and slabs for strength, stiffness and ductility, *Elsevier Science*, 2004.
8. Teng JG. Chen JF, Smith ST, Lam L. *FRP-Strengthened RC Structures*, England, John Wiley and sons, Ltd, 2002.
9. Maghsoudi AA, Akbarzadeh Bengar H. Acceptable lower bound of the ductility index and serviceability state of RC continuous beams strengthened with CFRP sheets, *Scientia Iranica*, **18**(2011) 36-44.
10. Lu F, Ayoub A. Evaluation of debonding failure of reinforced concrete girders strengthened in flexure with FRP laminates using finite element modeling, *Construction and Building Materials*, **25**(2011) 1963-79.
11. Teng J, Chen J, Smith S, Lam L. *RC Structures Strengthened With FRP Composites*,

Research Center for Advanced Technology in Structural Engineering, Department of Civil and Structural Engineering, Hong Kong, China: The Hong Kong Polytechnic University, 2000.
12. Smith ST, Teng JG. FRP-strengthened RC beams. I: review of debonding strength models, *Engineering Structures*, **24**(2002) 385-95.
13. ACI Committee 440. Guide for the design and construction of externally bonded FRP systems for strengthening concrete structures: American Concrete Institute, 2002.
14. ISIS Canada. Strengthening Reinforced Concrete Structures with Externally-bonded Fibre Reinforced Polymers. Vol. Design Manual, 2001.
15. Toutanji HZ, Zhao L, Zhang Y. Flexural behavior of reinforced concrete beams externally strengthened with CFRP sheets bonded with an inorganic matrix, *Engineering Structures*, **28**(2006) 557-66.
16. Lijuan L, Yongchang G, Feng L. Test analysis for FRC beams strengthened with externally bonded FRP sheets, *Construction and Building Materials*, **22**(2008) 315-23.